DMD Fast Forward. Published on February 2, 2018 as DOI: 10.1124/dmd.117.079194
This article has not been copyedited and formatted. The final version may differ from this version.

Manuscript title

Brain distribution of a novel MEK inhibitor E6201: implications in the treatment of melanoma brain metastases

Authors and affiliations

Gautham Gampa, Minjee Kim, Nicholas Cook-Rostie, Janice K. Laramy, Jann N. Sarkaria, Linda Paradiso, Louis DePalatis and William F. Elmquist

Brain Barriers Research Center, Department of Pharmaceutics, College of Pharmacy, University of Minnesota, Minneapolis, Minnesota, USA (GG, MK, NC, JKL, WFE)

Radiation Oncology, Mayo Clinic, Rochester, Minnesota, USA (JNS)

Strategia Therapeutics Inc., Spring, Texas, USA (LP, LD)

DMD Fast Forward. Published on February 2, 2018 as DOI: 10.1124/dmd.117.079194
This article has not been copyedited and formatted. The final version may differ from this version.

Running title

Pharmacokinetics, brain distribution and binding of E6201

Corresponding author

William F. Elmquist

Professor

Department of Pharmaceutics

University of Minnesota

308 Harvard Street SE

Minneapolis MN 55455

E-mail. elmqu011@umn.edu

Tel. +1(612) 625-0097

Fax. +1(612) 626-2125

Number of pages

Number of text pages: 26

Number of tables: 5

Number of figures: 6

Number of references: 45

Number of words in abstract: 242

Number of words in introduction: 654 (excluding in-text citations)

Number of words in discussion: 1511 (excluding in-text citations)

Supplemental table: none

Supplemental figure: 1

Abbreviations

AUC, area under the curve

BBB, blood-brain barrier

Bcrp, breast cancer resistance protein

CL, Clearance

CL/F, apparent clearance

Cmax, maximum drug concentration

CNS, central nervous system

DA, distribution advantage

fu, free (unbound) fraction

FVB, Friend leukemia virus strain B

GBM, Glioblastoma

HBD, hydrogen-bond donor

IC_{50}, half maximal inhibitory concentration

Kp, brain-to-plasma ratio

Kp,uu, unbound (free) brain-to-plasma ratio/ unbound partition coefficient

LC-MS/MS, liquid chromatography tandem mass spectroscopy

MAPK, mitogen-activated protein kinase

MBM, melanoma brain metastases

MDCKII, Madin-Darby canine kidney II

MR imaging, magnetic resonance imaging

NCA, noncompartmental analysis

PBS, phosphate buffered saline

OS, overall survival

P-gp, P-glycoprotein

PFS, progression-free survival

RED, rapid equilibrium dialysis

Tmax, time at the maximum drug concentration

TPSA, total polar surface area

Vd/F, apparent volume of distribution

Abstract

Clinically meaningful efficacy in the treatment of brain tumors, including melanoma brain metastases (MBM), requires selection of a potent inhibitor against a suitable target, and adequate drug distribution to target sites in the brain. Deregulated constitutive signaling of mitogen-activated protein kinase (MAPK) pathway has been frequently observed in melanoma, and MEK has been identified to be an important target. E6201 is a potent synthetic small molecule MEK inhibitor. The purpose of this study was to evaluate brain distribution of E6201, and examine the impact of active efflux transport at the BBB on the CNS exposure of E6201. In vitro studies utilizing transfected MDCKII cells indicate that E6201 is not a substrate of P-gp and Bcrp. In vivo studies also suggest a minimal involvement of P-gp and Bcrp in E6201's brain distribution. The total concentrations in brain were higher than in plasma, resulting in a brain-to-plasma AUC ratio (Kp) of 2.66 in wild-type mice. The brain distribution was modestly enhanced in *Mdr1a/b*$^{-/-}$, *Bcrp1*$^{-/-}$, and *Mdr1a/b*$^{-/-}$*Bcrp1*$^{-/-}$ knockout mice. The non-specific binding of E6201 was higher in brain compared to plasma. However, free drug concentrations in brain following 40 mg/kg intravenous dose reach levels that exceed reported in vitro IC_{50} values, suggesting that E6201 may be efficacious in inhibiting MEK-driven brain tumors. The brain distribution characteristics of E6201 makes it an attractive targeted agent for clinical testing in MBM, glioblastoma (GBM) and other CNS tumors that may be effectively targeted with inhibition of MEK signaling.

DMD Fast Forward. Published on February 2, 2018 as DOI: 10.1124/dmd.117.079194
This article has not been copyedited and formatted. The final version may differ from this version.

Introduction

Aberrant signaling of the mitogen-activated protein kinase (MAPK) pathway has been observed in about 80% of melanomas and various other types of cancers (Davies *et al.*, 2002). The discovery of activating mutations in the BRAF oncogene, observed in about 50% of melanoma patients, has led to significant advances in therapeutic options for metastatic melanoma (Hocker and Tsao, 2007; Samatar and Poulikakos, 2014). Melanoma patients treated with the newly developed molecularly targeted therapies, e.g., mutant BRAF inhibitors such as vemurafenib and dabrafenib, MEK inhibitors such as trametinib and cobimetinib, have shown improvements in overall survival (OS) (Falchook *et al.*, 2012; Long *et al.*, 2012; Cohen *et al.*, 2016; Margolin, 2016; Spagnolo *et al.*, 2016). However, initial responses are often followed by eventual relapse associated with resistance, occurring via mechanisms that cause subsequent hyperactivated downstream MEK signaling (Lito *et al.*, 2013; Samatar and Poulikakos, 2014). In patients with activating BRAF mutations, treatment with BRAF and MEK inhibitor combination showed improved responses compared to single-agent therapy and is an important treatment strategy (Flaherty *et al.*, 2012; Larkin *et al.*, 2014; Ribas *et al.*, 2014).

The burden of metastatic melanoma is projected to exceed 87000 new cases and 9700 deaths in the US in 2017 (Siegel *et al.*, 2017). Approximately 70% of patients with metastatic melanoma will develop brain metastases in their lifetime, and after a diagnosis of metastatic spread to the brain, the median overall survival (OS) is less than 6 months (Gupta *et al.*, 1997; Raizer *et al.*, Sloan *et al.*, 2009; Damsky *et al.*, 2014). Focal therapies with surgical resection and/or radiosurgery can effectively control an individual metastasis but the risk of developing subsequent brain metastases elsewhere in the brain exceeds 50%, which suggests that integrating these procedures with effective targeted therapies may provide significant clinical benefit (Fife, 2004). The successful treatment of brain tumors will need targeted therapies that are: (i) potent against its target, (ii) capable of penetrating an intact blood-brain barrier (BBB) replete with efflux transporters (Osswald *et al.*, 2016), and (iii) capable of reaching the protected tumor cells that are not clinically detectable upon contrast-enhancing MR imaging (Murrell *et al.*, 2015). Many small molecule molecularly-targeted therapies have limited ability to permeate an intact BBB, which in turn can limit their efficacy against brain tumors (Agarwal *et al.*, 2011; Gampa *et al.*, 2016, 2017). While the BBB at the core of larger brain tumors has been observed to be compromised, certain regions of such tumors and micrometastases can have a relatively intact BBB (Essig *et al.*, 2006; Murrell *et al.*, 2015; Osswald *et al.*, 2016). Active drug efflux, mainly by p-glycoprotein (P-gp) and breast cancer resistance protein (Bcrp), is a key mechanism responsible for limiting the

entry of various xenobiotics into the brain especially at sites with an intact BBB, including molecularly-targeted therapies approved for melanoma, such as vemurafenib, dabrafenib, trametinib and cobimetinib (Mittapalli *et al.*, 2012, 2013; Edna F Choo *et al.*, 2014; Vaidhyanathan *et al.*, 2014). As a consequence, drug delivery to tumor cells residing behind an intact BBB can be severely restricted, causing the establishment of a pharmacological sanctuary. There is a critical need to overcome issues related to brain drug delivery, and develop effective targeted therapies that can penetrate an intact BBB and reach the target sites on the tumor cells in the brain (Heffron, 2016).

E6201 (Figure 1) is a natural product-inspired synthetic non-allosteric kinase inhibitor that inhibits both MEK1 and FLT3 (Ikemori-Kawada *et al.*, 2012). E6201 is an ATP-competitive MEK inhibitor, in contrast to clinically approved drugs like trametinib and cobimetinib that are allosteric MEK inhibitors (Narita *et al.*, 2014). The binding affinity of E6201 has been shown to be identical for both the active and inactive forms of MEK1 (Goto *et al.*, 2009). The reported in vitro IC_{50} for E6201 against multiple melanoma cell lines (particularly BRAF mutant lines) was less than 100 nmol/L, indicating that E6201 exhibits potent activity against melanoma cells (Byron *et al.*, 2012; Narita *et al.*, 2014).

Given that melanoma has a high propensity to metastasize to the CNS, and inhibition of MEK has been recognized to be an important strategy in treating metastatic melanoma, testing the ability of E6201 to permeate an intact BBB would be essential. The purpose of this study was to determine the brain distribution of E6201 and evaluate the role of major BBB efflux proteins, P-gp and/or Bcrp in limiting the brain delivery of E6201, using mouse models. Such information can be valuable in evaluating the utility of this agent as an effective therapy for patients with melanoma brain metastases (MBM), and can inform future clinical trials. A brain penetrant MEK inhibitor would be particularly useful in patients with MBM, and as such would hold great promise for the treatment of metastatic melanoma.

DMD Fast Forward. Published on February 2, 2018 as DOI: 10.1124/dmd.117.079194
This article has not been copyedited and formatted. The final version may differ from this version.

Materials and methods

Chemicals

E6201 ((3S,4R,5Z,8S,9S,11E)-14-(ethylamino)-8,9,16-trihydroxy-3,4-dimethyl-3,4,9,10-tetrahydro-1H-2-benzoxacyclotetradecine-1,7(8H)-dione)) and ER807551 were kindly provided by Strategia Therapeutics Inc. (Houston, TX). [^{3}H]-Vinblastine was purchased from Moravek Biochemicals (La Brea, CA). [^{3}H]-Prazosin was purchased from PerkinElmer Life and Analytical Sciences (Waltham, MA). Ko143 [(3S,6S,12aS)-1,2,3,4,6,7,12,12a-octahydro-9-methoxy-6-(2-methylpropyl)-1,4-dioxopyrazino(1',2':1,6) pyrido(3,4-b)indole-3-propanoic acid 1,1-dimethylethyl ester] was purchased from Tocris Bioscience (Ellisville, MO). Zosuquidar [LY335979, (R)-4-([1aR, 6R,10bS]-1,2-difluoro-1,1a,6,10b-tetrahydrodibenzo-[a,e] cyclopropa [c]cycloheptan-6-yl)-([5-quinoloyloxy] methyl)-1-piperazine ethanol, trihydrochloride] was provided by Eli Lilly and Co. (Indianapolis, IN). All other chemicals used were of high-performance-liquid-chromatography or reagent grade and were obtained from Sigma-Aldrich (St. Louis, MO).

In Vitro Accumulation Studies

Polarized Madin-Darby canine kidney II (MDCKII) cells were used for performing in vitro accumulation studies. MDCKII-wild type and Bcrp1-transfected (MDCKII-Bcrp1) cell lines were a kind gift from Dr. Alfred Schinkel (The Netherlands Cancer Institute). MDCKII-wild type and gene encoding the human P-glycoprotein (MDR1)-transfected (MDCKII-MDR1) cell lines were kindly provided by Dr. Piet Borst (The Netherlands Cancer Institute). Cells were cultured in Dulbecco's modified Eagle's medium supplemented with 10% (v/v) fetal bovine serum and antibiotics (penicillin, 100 U/ml; streptomycin, 100 mg/ml; and amphotericin B, 250 ng/ml). Cells were grown in 25 mL tissue culture-treated flasks before seeding for the intracellular accumulation experiments and were maintained at 37°C in a humidified incubator with 5% carbon dioxide.

The intracellular accumulation of E6201 was performed in 12-well polystyrene plates (Corning Glassworks, Corning, NY). In brief, cells were seeded at a density of 2 x 10^5 cells and grown until ~80% confluent. On the day of experiment, the culture media was aspirated and the cells were washed two times with warm cell assay buffer (122 mM NaCl, 25 mM $NaHCO_3$, 10 mM glucose, 10 mM HEPES, 3 mM KCl, 2.5 mM $MgSO_4$, 1.8 mM $CaCl_2$, and 0.4 mM K_2HPO_4). The cells were then pre-incubated with cell assay buffer for 30 min, after which the buffer was aspirated and the experiment was initiated by adding 1 mL assay buffer containing 5 μM E6201 into each well with

DMD Fast Forward. Published on February 2, 2018 as DOI: 10.1124/dmd.117.079194
This article has not been copyedited and formatted. The final version may differ from this version.

further incubation for 60 minutes in an orbital shaker (ShelLab, Cornelius, OR) maintained at 37°C and 60 rpm. At the end of a 60-minute incubation, the experiment was ended by aspirating the E6201 solution followed by washing twice with ice-cold phosphate-buffered saline (PBS). The cell lysis was accomplished by adding 500 µL of 1% Triton-X100 to each well. When the inhibitor was used, it was included in both pre-incubation and accumulation steps. The concentration of E6201 in solubilized cell fractions was analyzed using liquid chromatography–tandem mass spectrometry (LC-MS/ MS) as described later, and was normalized to the protein content (BCA assay).

In vitro binding assays for determination of free (unbound) fraction of E6201 and trametinib

The free fraction of E6201 in plasma and brain were determined by performing rapid equilibrium dialysis (RED) experiments as per the protocol described by the manufacturer, with some modifications suggested in the literature (Cory Kalvass and Maurer, 2002; Friden *et al.*, 2007). RED base plate (Thermo Fisher Scientific), and single use RED inserts (Thermo Fisher Scientific) with 8 kDa molecular weight cut off (MWCO) were used for these experiments. Briefly, fresh plasma and brain homogenates (prepared in 3 volumes of PBS, w/v) isolated from wild-type FVB mice were used. E6201 stock in DMSO (1 mg/mL) was spiked in plasma and brain homogenate to obtain final concentrations of 10 µM (DMSO <1% of final volume). 300 µL of 10 µM E6201 spiked plasma/brain homogenate was placed in the sample chamber (donor), and 500 µL of phosphate buffered saline (1x PBS at pH 7.4; 100 mM sodium phosphate and 150 mM sodium chloride) was placed in buffer chamber (receiver) of the RED inserts in triplicates. The inserts were placed in a base plate, the assembly covered with sealing tape and incubated on an orbital shaker (ShelLab, Cornelius, OR) at 37^{o}C and 300 rpm for 4 hours (preliminary studies show that equilibrium is achieved by 4 hours). After dialysis, 150 µL of both plasma/brain homogenate and buffer were collected and the concentrations of E6201 were determined by LC-MS/MS. The Kp for trametinib has been previously reported in literature, but the fu was not available. So, RED experiments were performed to determine the free fractions of trametinib in plasma and brain, as described for E6201. The experiments were performed with a concentration of 2 µM trametinib in both plasma and brain matrices.

In vivo studies

Animals: Friend leukemia virus strain B (FVB) wild-type (WT), *Mdr1a/b*$^{-/-}$ (P-gp knockout), *Bcrp1*$^{-/-}$ (Bcrp knockout), and *Mdr1a/b*$^{-/-}$ *Bcrp1*$^{-/-}$ (triple knockout) mice of either sex (balanced) were used for all the in vivo studies (Taconic Farms, Germantown, NY). All mice used were 8-16 week-old adults, approximately 18 - 35 g, at the time of the experiments. Mice were maintained in a 12-hour light/dark cycle with unlimited access to food and

DMD Fast Forward. Published on February 2, 2018 as DOI: 10.1124/dmd.117.079194
This article has not been copyedited and formatted. The final version may differ from this version.

water. All studies carried out were in agreement with the guidelines set by Principles of Laboratory Animal Care (National Institutes of Health, Bethesda, MD), and approved by Institutional Animal Care and Use Committee (IACUC) at University of Minnesota.

Plasma and brain pharmacokinetics of E6201 after intravenous, intraperitoneal and oral administration: All dosing solutions were freshly prepared on the day of the experiment. E6201 dosing formulation was prepared by reconstituting lyophilized powder in single-use vials (received from Strategia Therapeutics Inc.), containing 60 mg E6201 and 3 g Captisol, with 8.5 mL sterile water for injection.

In the first set of studies, an intravenous (i.v.) bolus dose of 40 mg/kg E6201 (a dose previously used in efficacy studies, E6201 investigators brochure) was administered to FVB wild-type, *Mdr1a/b*$^{-/-}$, *Bcrp1*$^{-/-}$, and *Mdr1a/b*$^{-/-}$ *Bcrp1*$^{-/-}$ knockout mice via tail vein. Blood and brain samples were harvested at 0.083, 0.25, 0.5, 1, 2, 4 and 6 hours post-dose in a serial sacrifice (destructive sampling) design (n = 5 at each time point). At the desired sample collection time point, the animals were euthanized using a carbon dioxide chamber. Blood was collected by cardiac puncture in heparinized tubes. The whole brain was removed from the skull and washed with ice-cold distilled water, and superficial meninges were removed by blotting with tissue paper. Plasma was separated by centrifugation of whole blood at 3500 rpm and 4°C for 15 min. Both plasma and brain samples were stored at -80°C until further analysis for E6201 concentrations by LC-MS/MS. Brain concentrations were corrected for residual drug in brain vasculature assuming a vascular volume of 1.4% in mouse brain (Dai *et al.*, 2003).

In the second set of in vivo studies, 40 mg/kg E6201 was administered to FVB wild-type and *Mdr1a/b*$^{-/-}$ *Bcrp1*$^{-/-}$ knockout mice via intraperitoneal (i.p.) route. Blood and brain samples were harvested at 0.25, 0.5, 1, 2, 4 and 6 hours post-dose in a serial sacrifice design (n = 4 at each time point) as described for i.v. studies.

In the third study, 40 mg/kg E6201 was administered to FVB wild-type mice via oral gavage (p.o.). Blood and brain samples were harvested at 0.25, 0.5, 1, 2, 4 and 6 hours post-dose in a serial sacrifice design (n = 4 at each time point) as described for i.v. studies.

LC-MS/MS analysis

The concentrations of E6201 in all samples from in vitro and in vivo studies were determined using a specific and sensitive LC-MS/MS assay. E6201 and samples/solutions containing E6201 were protected from light in all experiments to avoid drug degradation. Brain samples were homogenized using a mechanical homogenizer

DMD Fast Forward. Published on February 2, 2018 as DOI: 10.1124/dmd.117.079194
This article has not been copyedited and formatted. The final version may differ from this version.

(PowerGen 125; Thermo Fisher Scientific, Waltham, MA) following the addition of three volumes of 5% bovine serum albumin (BSA) to obtain uniform homogenates. For analysis of unknowns, an aliquot of sample (cell lysate, cell assay buffer, PBS, plasma, or brain homogenate) was spiked with 50 ng of ER807551 as an internal standard and liquid-liquid extraction was performed by addition of 5-10 volumes of ethyl acetate, followed by vigorous shaking for 5 minutes and centrifugation at 7500 rpm and 4°C for 5 minutes. The organic layer was separated and transferred to microcentrifuge tubes, and dried under nitrogen gas. The dried powder was reconstituted in 100 µL of mobile phase and transferred into high-performance-liquid-chromatography glass vials with microinserts. Chromatographic analysis was performed using an AQUITY UPLC system (Waters, Milford, MA). The chromatographic separation was achieved by injection of 7.5 µL sample onto a C18 YMC-ODS-AM (3 µ particle size, 2.0 mm ID x 23 mm length; YMC America, USA) column. A gradient method was employed with mobile phase consisting of 0.1% formic acid in water as the aqueous component (A) and 0.1% formic acid in methanol as the organic component (B). The gradient was as follows: started with 35% B at 0 minutes, increased to 100% B by 0.5 minutes and maintained at 100% B up to 3.2 minutes, decreased to 35% B by 3.5 minutes and maintained at 35% B up to 7 minutes. The mobile phase was delivered at a constant flow rate of 0.3 mL/min.

The column effluent was monitored using a Micromass Quattro Ultima mass spectrometer (Waters, Milford, MA). The instrument was equipped with an electrospray interface, and controlled by the MassLynx (Version 4.1; Waters) data system. The samples were analyzed using an electrospray probe in the positive-ionization mode operating at a spray voltage of 2.5 kV for both E6201 and ER807551. Samples were introduced into the interface through a heated nebulized probe, in which the source temperature and desolvation temperature were set at 100°C and 400°C, respectively. The mass spectrometer was programmed to allow the $[MH]^+$ ions of E6201 and ER807551 at m/z ratios of 390.08 and 450.08, respectively, to pass through the first quadrupole (Q1) and into the collision cell (Q2). The collision energy was set at 20 V and 25 V for E6201 and ER807551, respectively. The daughter ions for E6201 (m/z 232) and ER807551 (m/z 273.96) were monitored through the third quadrupole (Q3). The retention times for E6201 and ER807551 were 1.11 and 1.12 minutes, respectively. The runtime was 7 minutes.

Pharmacokinetic analysis and calculations

Pharmacokinetic parameters from the concentration-time profiles in plasma and brain were obtained by non-compartmental analysis (NCA) performed using Phoenix WinNonlin version 6.4 (Certara USA, Inc., Princeton, NJ). The area under the concentration-time curves (AUC) for plasma (AUC_{plasma}) and brain (AUC_{brain}) were calculated

DMD Fast Forward. Published on February 2, 2018 as DOI: 10.1124/dmd.117.079194
This article has not been copyedited and formatted. The final version may differ from this version.

using the linear trapezoidal method. The standard errors around the means of AUC and Cmax were estimated using the sparse sampling module in WinNonlin (Nedelman and Jia, 1998).

Free (unbound) fraction (fu) in plasma and brain homogenate were calculated as the ratio of buffer to matrix concentrations of E6201 (Cory Kalvass and Maurer, 2002).

$$\text{fu, diluted} = \frac{\text{E6201 concentration in buffer (receiver)}}{\text{E6201 concentration in matrix (donor)}} \quad (Equation\ 1)$$

The fraction unbound for brain was determined from the measured fraction unbound in diluted brain homogenate (fu,diluted), using the following equation (Cory Kalvass and Maurer, 2002).

$$\text{fu, brain} = \frac{1/\text{D}}{(1/\text{fu, diluted} - 1) + 1/\text{D}} \quad (Equation\ 2)$$

where D (equal to 4) represents the dilution factor, accounting for the diluted brain homogenate.

The recovery was estimated using the equation,

$$\text{Recovery (\%)} = \frac{(\text{donor mass} + \text{receiver mass})\text{after dialysis}}{\text{donor mass, before dialysis}} \text{ x } 100 \quad (Equation\ 3)$$

The brain-to-plasma ratio (Kp) was calculated as the ratio of AUC_{brain} to AUC_{plasma}.

$$\text{Kp} = \frac{\text{AUCbrain}}{\text{AUCplasma}} \quad (Equation\ 4)$$

A comparison of relative drug exposure in the brain between wild-type and knockout (*Mdr1a/b*$^{-/-}$, *Bcrp1*$^{-/-}$, *and Mdr1a/b*$^{-/-}$ *Bcrp1*$^{-/-}$) mice was made using the distribution advantage (DA).

$$\text{DA} = \frac{\text{Kp}, knockout}{\text{Kp}, wild\ type} \quad (Equation\ 5)$$

The unbound partition coefficient (Kp,uu) was calculated for the four genotypes using the equation,

$$\text{Kp, uu} = \frac{\text{AUCbrain x fu, brain}}{\text{AUCplasma x fu, plasma}} \quad (Equation\ 6)$$

Statistical Analysis

GraphPad Prism version 6.04 (GraphPad, L Jolla, CA) software was used for the statistical analysis. The sample sizes used were based on previous work and were determined based on approximately 80% power to detect 50% difference between groups. Data from all experiments are represented as mean ± standard deviation (S.D.) or mean ± standard error of the mean (S.E.M) unless otherwise indicated. Comparisons between two groups were made using

an unpaired t-test. Comparisons between multiple groups were made using one-way analysis of variance (ANOVA), followed by Bonferroni's multiple comparison test. A significance level of $P < 0.05$ was used for all statistical analysis.

DMD Fast Forward. Published on February 2, 2018 as DOI: 10.1124/dmd.117.079194
This article has not been copyedited and formatted. The final version may differ from this version.

Results

In vitro accumulation of E6201 in MDCKII-Bcrp1 and MDCKII-MDR1 cells

The intracellular accumulation of E6201 in MDCKII wild-type, Bcrp1-transfected, and MDR1-transfected cell lines is summarized in Figure 2. [^{3}H]-Prazosin and [^{3}H]-vinblastine were used as positive controls for Bcrp1 and MDR1, respectively. As expected, the cellular accumulation of [^{3}H]-prazosin was significantly lower as compared with wild-type controls (WT: 100±29%; Bcrp1: 25±5%; $P<0.05$). Similarly, the cellular accumulation of [^{3}H]-vinblastine was also significantly lower when compared with wild-type controls (WT: 100±31%; MDR1: 7±1%; $P<0.01$). These results validate the significant elevation of efflux transporter activity in the relevant transfected cell lines. In the same experiment, incubation with 5 μM E6201 showed that the accumulation of E6201 was not significantly different in Bcrp1 cells (Bcrp: 107±29%; WT: 100±29%), and in MDR1 cells (MDR1: 89±16%; WT: 100±9%) when compared with corresponding wild-type controls. The addition of 0.2 μM Ko143, a specific Bcrp1 inhibitor, to the Bcrp1 cells and 1 μM LY335979, a specific MDR1 inhibitor, to MDR1 cells did not lead to significant differences in intracellular accumulation when compared to transfected cells without inhibitor. These data indicate that E6201 is not a substrate for either P-gp or Bcrp1.

Determination of free (unbound) fraction of E6201 and trametinib

In vitro rapid equilibrium dialysis was used for the determination of free fraction (equations 1 and 2) in plasma and brain. The free fraction (fu) for E6201 in plasma was determined to be 2.63 ± 0.18% and the mass balance recovery of the experiment was 94.04 ± 3.32% (Table 1). The fu for E6201 in brain was found to be 0.14 ± 0.02% and the mass balance recovery was 113.20 ± 9.50% (Table 1). The fu for trametinib in plasma was found to be 0.21 ± 0.03% and the mass balance recovery of the experiment was 99.9% ± 8.42% (Table 1). The fu for trametinib in brain was determined to be 0.21 ± 0.02% and the mass balance recovery was 106.56 ± 2.35% (Table 1). The estimated fu values were used for the determination of unbound partition coefficient, Kp,uu.

Plasma and brain pharmacokinetics following intravenous, intraperitoneal and oral E6201 administration

The pharmacokinetic parameters for E6201 were determined in FVB wild-type and transporter deficient (knockout) mice following various routes of E6201 administration. The brain and plasma concentration time profiles and brain-to-plasma ratio profiles in FVB wild-type, *Mdr1a/b$^{-/-}$, Bcrp1$^{-/-}$, and Mdr1a/b$^{-/-}$ Bcrp1$^{-/-}$* mice following a single intravenous bolus dose of 40 mg/kg E6201 are as shown in Figure 3. The total plasma E6201 concentrations (Figure

3A) were similar between the four genotypes at any given time point. The total brain E6201 concentrations (Figure 3B) at the indicated time points were higher than the total plasma concentrations in all the four genotypes. Table 2 summarizes the estimated pharmacokinetic parameters in the four genotypes of mice studied. There were no statistically significant differences between the wild-type plasma AUC and any of the transporter knockout plasma AUCs. The estimated AUCs in the brain for *Mdr1a/b*$^{-/-}$*, Bcrp1*$^{-/-}$*, and Mdr1a/b*$^{-/-}$ *Bcrp1*$^{-/-}$ mice were significantly higher when compared with the AUC in wild-type mice ($P<0.05$). The observed systemic clearance and volume of distribution were similar in the wild-type and knockout mice. The brain-to-plasma AUC ratios (Kp, equation 4) in the wild-type, *Mdr1a/b*$^{-/-}$*, Bcrp1*$^{-/-}$*, and Mdr1a/b*$^{-/-}$ *Bcrp1*$^{-/-}$ mice were 2.66, 4.37, 3.72 and 5.40, respectively. A comparison of relative drug exposure in the brain between wild-type and knockout (*Mdr1a/b*$^{-/-}$*, Bcrp1*$^{-/-}$*, and Mdr1a/b*$^{-/-}$ *Bcrp1*$^{-/-}$) mice was made using the distribution advantage (DA), which is defined as the Kp in knockout mice normalized by the Kp in wild-type mice (equation 5). The DA in *Mdr1a/b*$^{-/-}$*, Bcrp1*$^{-/-}$*, and Mdr1a/b*$^{-/-}$ *Bcrp1*$^{-/-}$ mice were 1.64, 1.39 and 2.03, suggesting minimal involvement of P-gp and Bcrp in limiting the brain distribution of E6201. The extent of distribution of free drug is represented by term "Kpuu" and can be defined as the ratio of the unbound drug exposure in the brain over the unbound drug exposure in plasma (equation 6). The Kp,uu in the wild-type, *Mdr1a/b*$^{-/-}$*, Bcrp1*$^{-/-}$*, and Mdr1a/b*$^{-/-}$ *Bcrp1*$^{-/-}$ mice were 0.14, 0.24, 0.20 and 0.29, respectively.

The concentration time profiles and brain-to-plasma ratio profiles in FVB wild-type *and Mdr1a/b*$^{-/-}$ *Bcrp1*$^{-/-}$ mice following a single intraperitoneal dose of 40 mg/kg E6201 are shown in Figure 4. The estimated pharmacokinetic parameters are summarized in Table 3. There was no statistically significant difference between the wild-type plasma AUC and *Mdr1a/b*$^{-/-}$ *Bcrp1*$^{-/-}$ plasma AUC. The AUC in the brain for *Mdr1a/b*$^{-/-}$ *Bcrp1*$^{-/-}$ mice was significantly higher when compared to the AUC in wild-type mice ($P<0.05$). The Kp in wild-type *and Mdr1a/b*$^{-/-}$ *Bcrp1*$^{-/-}$ mice were 2.2 and 3.83, respectively. The Kp,uu values in wild-type *and Mdr1a/b*$^{-/-}$ *Bcrp1*$^{-/-}$ mice were 0.12 and 0.21, respectively. The absolute bioavailability (F) following i.p. administration was found to be 0.95.

The concentration time profiles and brain-to-plasma ratio profile in FVB wild-type mice following single oral dose of 40 mg/kg E6201 are shown in Figure 5. The estimated pharmacokinetic parameters are summarized in Table 4. The Kp and Kp,uu were found to be 2.35 and 0.13, respectively. The absolute bioavailability following p.o. administration was 0.39.

DMD Fast Forward. Published on February 2, 2018 as DOI: 10.1124/dmd.117.079194
This article has not been copyedited and formatted. The final version may differ from this version.

Discussion

The approved small molecule targeted therapies for melanoma; inhibitors of MAP kinase signaling (BRAF inhibitors, vemurafenib and dabrafenib; MEK inhibitors, trametinib and cobimetinib) and large molecule immune checkpoint inhibitors (CTLA-4 inhibitors such as ipilimumab, and PD-1 inhibitors such as nivolumab) have shown improvements in overall survival (OS) and progression-free survival (PFS) by a few months in patients with MBM (Falchook *et al.*, 2012; Long *et al.*, 2012; Dummer *et al.*, 2014; Cohen *et al.*, 2016; Margolin, 2016; Spagnolo *et al.*, 2016). While encouraging (Bates, 2013), it is still difficult to treat advanced metastatic disease that has spread to the brain. The modest efficacy in patients with MBM may be related to both inadequate drug delivery and specific brain microenvironment driven changes in gene expression. Previous studies have shown that vemurafenib, dabrafenib, trametinib and cobimetinib have limited brain distribution due to active efflux by Bcrp and/or P-gp (Mittapalli *et al.*, 2012, 2013; Edna F Choo *et al.*, 2014; Vaidhyanathan *et al.*, 2014).

E6201, a novel MEK inhibitor, may be beneficial in treatment of melanoma either in combination with a BRAF inhibitor or as a single agent. In the current study, we investigated brain distribution of E6201 in mice, examined the role of efflux transport on brain distribution, and determined its free fraction in plasma and brain. The results help us understand if E6201 can distribute across the BBB to achieve therapeutically active levels, and also allow us to compare E6201's brain distribution profile with currently available MEK inhibitors. To our knowledge, this is the first report of the brain distribution and active efflux of E6201.

In vitro intracellular accumulation studies in transfected MDCKII cells overexpressing either murine Bcrp or human P-gp, strongly suggest that E6201 is not a substrate of Bcrp or P-gp. The intracellular E6201 concentrations were not different between wild-type and Bcrp1-/MDR1-transfected cells, and also in Bcrp1- and MDR1-transfected cells treated with and without specific inhibitor of transporter (Figure 2). Moreover, directional flux studies showed that E6201 was unlikely to be a substrate of P-gp (E6201 investigators brochure). Subsequent experiments tested the influence of Bcrp and/or P-gp on brain distribution of E6201 in vivo.

In vivo pharmacokinetic experiments following 40 mg/kg single intravenous bolus dose of E6201 indicate that total concentrations in brain were higher than that in plasma at all measured time points in the four genotypes, while plasma concentrations were similar (Figure 3). Consequently, observed AUCs in brain were higher than AUCs in plasma, as can be recognized from the brain-to-plasma AUC ratios (Kp) of 2.66, 4.37, 3.72 and 5.40 in wild-type,

DMD Fast Forward. Published on February 2, 2018 as DOI: 10.1124/dmd.117.079194
This article has not been copyedited and formatted. The final version may differ from this version.

Mdr1a/b$^{-/-}$*, Bcrp1*$^{-/-}$*, and Mdr1a/b*$^{-/-}$ *Bcrp1*$^{-/-}$ mice, respectively (Table 2). While plasma AUCs are not significantly different, brain AUCs are significantly higher in knockouts compared to wild-type mice. This indicates that P-gp and Bcrp may play a role in limiting E6201's brain delivery; however, the increase in exposure is minimal (2-fold in *Mdr1a/b*$^{-/-}$ *Bcrp1*$^{-/-}$ mice) when compared to many substrates reported in literature, for instance cobimetinib (30-fold in *Mdr1a/b*$^{-/-}$ *Bcrp1*$^{-/-}$ mice (Edna F Choo *et al.*, 2014)) and trametinib (5-fold in *Mdr1a/b*$^{-/-}$ *Bcrp1*$^{-/-}$ mice (Vaidhyanathan *et al.*, 2014)). A possibility for the modest increase in Kp (≤2-fold), given the in vitro results, could be related to changes in transporter expression in knockout mice. Though a change in expression could be possible for some unknown transporter, it is unlikely here, given the results of transporter, receptor, and tight junction proteomic analysis in wild-type compared to *Mdr1a/b*$^{-/-}$ and/or *Bcrp1*$^{-/-}$ mice (Agarwal *et al.*, 2012) indicated no change in expression of BBB proteins. Nevertheless, these results show that E6201, for a molecularly-targeted agent, has brain distribution characteristics that are minimally influenced by Bcrp and P-gp efflux at the BBB.

The brain partitioning following i.p. and p.o. administration of E6201 at the same dose was similar to that observed in i.v. studies. The absolute bioavailability (F) of E6201 was higher following i.p dosing compared to p.o. dosing (F=0.95, i.p., F=0.39, p.o.; Table 3, Table 4). Consistent with in vitro results, in vivo studies characterizing the brain exposure of E6201 demonstrate that neither Bcrp nor P-gp show a marked involvement in limiting the brain delivery of E6201.

In vitro rapid equilibrium dialysis experiments indicate that E6201 exhibits higher non-specific binding in brain compared to plasma, possibly related to lipophilic brain environment, with free fractions (fu) of 0.14% and 3.4%, respectively (Table 1). The fu values were used to estimate the unbound partition coefficients (Kp,uu) in wild-type, *Mdr1a/b*$^{-/-}$*, Bcrp1*$^{-/-}$*, and Mdr1a/b*$^{-/-}$ *Bcrp1*$^{-/-}$ mice, 0.14, 0.24, 0.2 and 0.29, respectively, following i.v. dosing (Table 2). The Kp,uu values in all four genotypes of mice were less than one indicating a distribution disequilibrium (Di *et al.*, 2013; Summerfield *et al.*, 2016). It is likely that E6201 has a high passive permeability in the absence of active efflux, since it is a relatively small molecule (389.45 g/mol), highly lipophilic (xlogP3 = 3.3 (Pubchem), logP = 3.63 (E6201 investigators brochure)), and not significantly charged at physiological pH (pKa of basic nitrogen = 8.8 (E6201 investigators brochure)). Also, it can be seen from the brain-to-plasma ratio plot for the four genotypes (Figure 3C) that an equilibrium between brain and plasma concentrations is achieved rapidly (~0.5 hr) suggesting a high rate into brain. Given these observations, it is possible that Kp,uu less than unity is related to efflux

DMD Fast Forward. Published on February 2, 2018 as DOI: 10.1124/dmd.117.079194
This article has not been copyedited and formatted. The final version may differ from this version.

transporter(s) other than Bcrp and P-gp are influencing E6201's brain delivery, especially given that Kp,uu in *Mdr1a/b*$^{-/-}$ *Bcrp1*$^{-/-}$ mice is also less than unity.

The average free drug concentrations in wild-type mice were determined at measured time points to obtain the free concentration-time profile. The free concentrations were then compared to in vitro potency estimates in melanoma cell lines to evaluate the potential of E6201 for treatment of MBM. The free concentrations in brain reached levels higher than the reported IC_{50} value (IC_{50} = 43.7 nmol/L, SK-MEL-28 melanoma cell line; E6201 investigators brochure), suggesting that E6201 may show efficacy in treatment of MEK-driven brain tumors (Figure 6). Also, since the IC_{50} measurements employed total and not free concentrations in media, the free IC_{50} can be expected to be even lower, giving further credence to the idea that adequate delivery may be achieved in vivo. Given such insights, it would be valuable to conduct efficacy studies with E6201 in preclinical models of MBM as a next step to better understand in vivo efficacy, and lead to clinical trials.

The unique macrocyclic structure of E6201 may enhance its brain penetration by avoiding active efflux via Bcrp and P-gp. A macrocyclic structure facilitates a reduction in rotatable bonds, reported to positively correlate with improved brain penetration by lessening active efflux (Heffron, 2016). Also, of at least equal, and probably greater, significance is the opportunity for formation of intramolecular hydrogen bonds that can effectively mask hydrogen-bond donors (HBD), which have a profound correlation with likelihood of transporter mediated efflux (Heffron, 2016). The 3-dimensional x-ray crystal structure of E6201 bound to MEK (see http://www.rcsb.org/pdb/explore.do?structureId=5HZE) shows that each of the alcohol/phenol "OH" groups are capable of intramolecular hydrogen bonding, thereby allowing effective masking of 3 of the 4 available HBDs, essentially leaving only 1 effective HBD. Such observations have been reported for other targeted agents such as lorlatinib (ALK inhibitor) and AZD3759 (EGFR inhibitor) (Johnson *et al.*, 2014; Zeng *et al.*, 2015). Recent literature highlights the fact that an optimal balance of physicochemical properties is necessary to achieve adequate distribution to brain, and drugs having low molecular weight, fewer rotatable bonds, low total polar surface area (TPSA), and fewer HBDs are expected to have better CNS penetration (Rankovic, 2015; Heffron, 2016; Wager *et al.*, 2016). The combination of few rotatable bonds and few effective HBDs readily explains how E6201 achieves significant brain distribution.

In the context of brain tumors, it is important to note that the approved MEK inhibitors, trametinib and cobimetinib, show limited brain distribution due to active efflux. The Kp for trametinib and cobimetinib in wild-type mice were

0.15 and 0.32, respectively (Table 5). As evident from the Kp of 2.66 in wild-type mice, the total concentrations for E6201 are higher in brain compared to plasma, unlike for trametinib and cobimetinib. Given that the three MEK inhibitors are highly protein bound, Kp,uu for E6201 is much higher than that of cobimetinib and similar to that of trametinib (Table 5). The brain distribution profile of E6201 makes it an attractive MEK inhibitor for the treatment of MBM, with potential for achieving improved treatment responses.

The development of targeted agents inhibiting the MAPK pathway and immunotherapies has led to major advances in the treatment of patients with metastatic melanoma. However, it is crucial to realize the challenges that still remain in delivering the molecularly-targeted agents to tumor cells in the brain that may be growing behind an intact BBB. Both the brain microenvironment-driven changes in genetic expression leading to resistance and CNS drug delivery issues need to be addressed to achieve a clinically meaningful response in MBM and other brain tumors. Though single agent treatment may show responses, there is a need to test rational combinations (e.g., a BRAF inhibitor and MEK inhibitor to better inhibit MAPK pathway; a BRAF/MEK inhibitor and a PI3K/mTOR inhibitor to inhibit both MAPK and PI3K pathways) to tackle issues of resistance to therapy. When using combinations, it is important to examine CNS distribution of all agents in the combination regimen since all administered drugs should adequately reach the target site in brain to achieve desired responses and minimize emergence of resistance. Despite the remarkable progress, there remains a need to develop better therapies for MBMs, and drug delivery across the BBB is one crucial factor that requires attention to fulfill this goal.

Acknowledgements

The authors thank Jim Fisher, Clinical Pharmacology Analytical Laboratory, University of Minnesota, for his support in the development of the LC-MS/MS assays. The authors would also like to thank Timothy Heffron from Genentech Inc., for his valuable input.

Authorship contributions

Participated in research design: Gampa, Kim, Laramy, Sarkaria, Paradiso, DePalatis, Elmquist.

Conducted experiments: Gampa, Kim, Cook-Rostie, Laramy.

Performed data analysis: Gampa, Kim, Laramy, Elmquist.

Wrote or contributed to the writing of the manuscript: Gampa, Laramy, Sarkaria, Paradiso, DePalatis, Elmquist.

References

Agarwal S, Sane R, Oberoi R, Ohlfest JR, and Elmquist WF (2011) Delivery of molecularly targeted therapy to malignant glioma, a disease of the whole brain. *Expert Rev Mol Med* **13**:e17.

Agarwal S, Uchida Y, Mittapalli RK, Sane R, Terasaki T, and Elmquist WF (2012) Quantitative Proteomics of Transporter Expression in Brain Capillary Endothelial Cells Isolated from P-Glycoprotein (P-gp), Breast Cancer Resistance Protein (Bcrp), and P-gp / Bcrp Knockout Mice □ ABSTRACT :

Bates SE (2013) A sea change in melanoma. *Clin Cancer Res* **19**:5282.

Byron S a, Loch DC, Wellens CL, Wortmann A, Wu J, Wang J, Nomoto K, and Pollock PM (2012) Sensitivity to the MEK inhibitor E6201 in melanoma cells is associated with mutant BRAF and wildtype PTEN status. *Mol Cancer* **11**:75.

Cohen J V., Tawbi H, Margolin KA, Amravadi R, Bosenberg M, Brastianos PK, Chiang VL, de Groot J, Glitza IC, Herlyn M, Holmen SL, Jilaveanu LB, Lassman A, Moschos S, Postow MA, Thomas R, Tsiouris JA, Wen P, White RM, Turnham T, Davies MA, and Kluger HM (2016) Melanoma central nervous system metastases: current approaches, challenges, and opportunities. *Pigment Cell Melanoma Res* **29**:627–642.

Cory Kalvass J, and Maurer TS (2002) Influence of nonspecific brain and plasma binding on CNS exposure: implications for rational drug discovery. *Biopharm Drug Dispos* **23**:327–338, John Wiley & Sons, Ltd.

Dai H, Marbach P, Lemaire M, Hayes M, and Elmquist WF (2003) Distribution of STI-571 to the brain is limited by P-glycoprotein-mediated efflux. *J Pharmacol Exp Ther* **304**:1085–1092.

Damsky WE, Theodosakis N, and Bosenberg M (2014) Melanoma metastasis: new concepts and evolving paradigms. *Oncogene* **33**:2413–2422, Nature Publishing Group.

Davies H, Bignell GR, Cox C, Stephens P, Edkins S, Clegg S, Teague J, Woffendin H, Garnett MJ, Bottomley W, Davis N, Dicks E, Ewing R, Floyd Y, Gray K, Hall S, Hawes R, Hughes J, Kosmidou V, Menzies A, Mould C, Parker A, Stevens C, Watt S, Hooper S, Wilson R, Jayatilake H, Gusterson BA, Cooper C, Shipley J, Hargrave D, Pritchard-Jones K, Maitland N, Chenevix-Trench G, Riggins GJ, Bigner DD, Palmieri G, Cossu A, Flanagan A, Nicholson A, Ho JWC, Leung SY, Yuen ST, Weber BL, Seigler HF, Darrow TL, Paterson H, Marais R, Marshall CJ, Wooster R, Stratton MR, and Futreal PA (2002) Mutations of the BRAF gene in human cancer. *Nature* **417**:949–954.

Di L, Rong H, and Feng B (2013) Demystifying brain penetration in central nervous system drug discovery.

Dummer R, Goldinger SM, Turtschi CP, Eggmann NB, Michielin O, Mitchell L, Veronese L, Hilfiker PR, Felderer L, and Rinderknecht JD (2014) Vemurafenib in patients with BRAFV600 mutation-positive melanoma with symptomatic brain metastases: Final results of an open-label pilot study. *Eur J Cancer* **50**:611–621.

Edna F Choo, Ly J, Chan J, Shahidi-Latham SK, Messick K, Plise E, Quiason CM, and Yang L (2014) Cobimetinib_Role of P- Glycoprotein on the Brain Penetration and Brain Pharmacodynamic Activity of the MEK Inhibitor Cobimetinib. *Mol Pharm* **11**:4199–4207.

Essig M, Weber M-A, von Tengg-Kobligk H, Knopp M V, Yuh WTC, and Giesel FL (2006) Contrast-enhanced magnetic resonance imaging of central nervous system tumors: agents, mechanisms, and applications. *Top Magn Reson Imaging* **17**:89–106.

Falchook GS, Long G V., Kurzrock R, Kim KB, Arkenau TH, Brown MP, Hamid O, Infante JR, Millward M, Pavlick AC, O'Day SJ, Blackman SC, Curtis CM, Lebowitz P, Ma B, Ouellet D, and Kefford RF (2012) Dabrafenib in patients with melanoma, untreated brain metastases, and other solid tumours: A phase 1 dose-escalation trial. *Lancet* **379**:1893–1901.

Fife KM (2004) Determinants of Outcome in Melanoma Patients With Cerebral Metastases. *J Clin Oncol* **22**:1293–1300.

Flaherty KT, Infante JR, Daud A, Gonzalez R, Kefford RF, Sosman J, Hamid O, Schuchter L, Cebon J, Ibrahim N, Kudchadkar R, Burris HA, Falchook G, Algazi A, Lewis K, Long G V., Puzanov I, Lebowitz P, Singh A, Little S, Sun P, Allred A, Ouellet D, Kim KB, Patel K, and Weber J (2012) Combined BRAF and MEK Inhibition in Melanoma with BRAF V600 Mutations. *N Engl J Med* **367**:1694–1703.

Friden M, Gupta A, Antonsson M, Bredberg U, and Hammarlund-Udenaes M (2007) In Vitro Methods for Estimating Unbound Drug Concentrations in the Brain Interstitial and Intracellular Fluids. *Drug Metab Dispos* **35**:1711–1719.

Gampa G, Vaidhyanathan S, Sarkaria JN, and Elmquist WF (2017) Perspective Drug delivery to melanoma brain metastases: Can current challenges lead to new opportunities? *Pharmacol Res* **123**:10–25.

Gampa G, Vaidhyanathan S, Wilken-Resman B, Parrish KE, Markovic SN, Sarkaria JN, and Elmquist WF (2016) Challenges in the Delivery of Therapies to Melanoma Brain Metastases. *Curr Pharmacol Reports* **2**:309–325.

Goto M, Chow J, Muramoto K, Chiba K, Yamamoto S, Fujita M, Obaishi H, Tai K, Mizui Y, Tanaka I, Young D, Yang H, Wang YJ, Shirota H, and Gusovsky F (2009) 1 , 7 (8 H) -dione], a Novel Kinase Inhibitor of Mitogen-Activated Protein Kinase / Extracellular Signal-Regulated Kinase Kinase (MEK) -1 and MEK Kinase-1 : In Vitro Characterization of Its Anti-Inflammatory and Antihyperproliferative Activities. *J Pharmacol Exp Ther* **331**:485–495.

Gupta G, Robertson AG, and MacKie RM (1997) Cerebral metastases of cutaneous melanoma. *Br J Cancer* **76**:256–9.

Heffron TP (2016) Small Molecule Kinase Inhibitors for the Treatment of Brain Cancer. *J Med Chem* **59**:10030–10066.

Hocker T, and Tsao H (2007) Ultraviolet radiation and melanoma: A systemic review and analysis of reported sequence variants. *Hum Mutat* **28**:578–588.

Ikemori-Kawada M, Inoue A, Goto M, Wang YJ, and Kawakami Y (2012) Docking simulation study and kinase selectivity of f152A1 and its analogs. *J Chem Inf Model* **52**:2059–2068.

Johnson TW, Richardson PF, Bailey S, Brooun A, Burke BJ, Collins MR, Cui JJ, Deal JG, Deng YL, Dinh D, Engstrom LD, He M, Hoffman J, Hoffman RL, Huang Q, Kania RS, Kath JC, Lam H, Lam JL, Le PT, Lingardo L, Liu W, McTigue M, Palmer CL, Sach NW, Smeal T, Smith GL, Stewart AE, Timofeevski S, Zhu H, Zhu J, Zou HY, and Edwards MP (2014) Discovery of (10 R)-7-Amino-12-fluoro-2,10,16-trimethyl-15-oxo-10,15,16,17- tetrahydro- 2H -8,4-(metheno)pyrazolo[4,3- h][2,5,11]- benzoxadiazacyclotetradecine-3-carbonitrile (PF-06463922), a macrocyclic inhibitor of anaplastic lymphoma kinase (ALK) and . *J Med Chem* **57**:4720–4744.

Larkin J, Ascierto PA, Dréno B, Atkinson V, Liszkay G, Maio M, Mandalà M, Demidov L, Stroyakovskiy D, Thomas L, de la Cruz-Merino L, Dutriaux C, Garbe C, Sovak MA, Chang I, Choong N, Hack SP, McArthur GA, and Ribas A (2014) Combined Vemurafenib and Cobimetinib in *BRAF* -Mutated Melanoma. *N Engl J Med* **371**:1867–1876.

Lito P, Rosen N, and Solit DB (2013) Tumor adaptation and resistance to RAF inhibitors. *Nat Med* **19**:1401–1409.

Long G V., Trefzer U, Davies MA, Kefford RF, Ascierto PA, Chapman PB, Puzanov I, Hauschild A, Robert C, Algazi A, Mortier L, Tawbi H, Wilhelm T, Zimmer L, Switzky J, Swann S, Martin AM, Guckert M, Goodman V, Streit M, Kirkwood JM, and Schadendorf D (2012) Dabrafenib in patients with Val600Glu or Val600Lys BRAF-mutant melanoma metastatic to the brain (BREAK-MB): A multicentre, open-label, phase 2 trial. *Lancet Oncol* **13**:1087–1095.

Margolin K (2016) The Promise of Molecularly Targeted and Immunotherapy for Advanced Melanoma. *Curr Treat Options Oncol* **17**:1–14, Current Treatment Options in Oncology.

Mittapalli RK, Vaidhyanathan S, Dudek AZ, and Elmquist WF (2013) Mechanisms Limiting Distribution of the Threonine-Protein Kinase B-RaF V600E Inhibitor Dabrafenib to the Brain: Implications for the Treatment of Melanoma Brain Metastases. *J Pharmacol Exp Ther J Pharmacol Exp Ther* **344**:655–664.

Mittapalli RK, Vaidhyanathan S, Sane R, and Elmquist WF (2012) Impact of P-Glycoprotein (ABCB1) and Breast Cancer Resistance Protein (ABCG2) on the Brain Distribution of a Novel BRAF Inhibitor: Vemurafenib (PLX4032). *J Pharmacol Exp Ther* **342**:33–40.

Murrell DH, Hamilton AM, Mallett CL, van Gorkum R, Chambers AF, and Foster PJ (2015) Understanding Heterogeneity and Permeability of Brain Metastases in Murine Models of HER2-Positive Breast Cancer Through Magnetic Resonance Imaging: Implications for Detection and Therapy. *Transl Oncol* **8**:176–184, The Authors.

Narita Y, Okamoto K, Kawada MI, Takase K, Minoshima Y, Kodama K, Iwata M, Miyamoto N, and Sawada K (2014) Novel ATP-Competitive MEK Inhibitor E6201 Is Effective against Vemurafenib-Resistant Melanoma Harboring the MEK1-C121S Mutation in a Preclinical Model. *Mol Cancer Ther*, doi: 10.1158/1535-7163.MCT-13-0667.

Nedelman JR, and Jia X (1998) An extension of Satterthwaite's approximation applied to pharmacokinetics. *J*

Biopharm Stat **8**:317–328.

Osswald M, Blaes J, Liao Y, Solecki G, Go mmel M, Berghoff AS, Salphati L, Wallin JJ, Phillips HS, Wick W, and Winkler F (2016) Impact of Blood-Brain Barrier Integrity on Tumor Growth and Therapy Response in Brain Metastases. *Clin Cancer Res* **22**:6078–6087.

Raizer JJ, Hwu W-J, Panageas KS, Wilton A, Baldwin DE, Bailey E, von Althann C, Lamb LA, Alvarado G, Bilsky MH, and Gutin PH (2008) Brain and leptomeningeal metastases from cutaneous melanoma: Survival outcomes based on clinical features. *Neuro Oncol* **10**:199–207.

Rankovic Z (2015) CNS Drug Design: Balancing Physicochemical Properties for Optimal Brain Exposure. *J Med Chem* **58**:2584–2608.

Ribas A, Gonzalez R, Pavlick A, Hamid O, Gajewski TF, Daud A, Flaherty L, Logan T, Chmielowski B, Lewis K, Kee D, Boasberg P, Yin M, Chan I, Musib L, Choong N, Puzanov I, and McArthur GA (2014) Combination of vemurafenib and cobimetinib in patients with advanced BRAFV600-mutated melanoma: A phase 1b study. *Lancet Oncol* **15**:954–965, Elsevier Ltd.

Samatar AA, and Poulikakos PI (2014) Targeting RAS–ERK signalling in cancer: promises and challenges. *Nat Rev Drug Discov* **13**:928–942, Nature Publishing Group.

Siegel RL, Miller KD, and Jemal A (2017) Cancer statistics, 2017. *CA Cancer J Clin* **67**:7–30.

Sloan AE, Nock CJ, and Einstein DB (2009) Diagnosis and treatment of melanoma brain metastasis: a literature review. *Cancer Control* **16**:248–55.

Spagnolo F, Picasso V, Lambertini M, Ottaviano V, Dozin B, and Queirolo P (2016) Survival of patients with metastatic melanoma and brain metastases in the era of MAP-kinase inhibitors and immunologic checkpoint blockade antibodies: A systematic review. *Cancer Treat Rev* **45**:38–45, Elsevier Ltd.

Summerfield SG, Zhang Y, and Liu H (2016) Examining the Uptake of CNS Drugs and Candidates Across the Blood-Brain Barrier. *J Pharmacol Exp Ther* 294–305.

Vaidhyanathan S, Mittapalli RK, Sarkaria JN, and Elmquist WF (2014) Factors Influencing the CNS Distribution of a Novel MEK-1/2 inhibitor: Implications for Combination Therapy for Melanoma Brain Metastases. *Drug Metab Dispos* **42**:1292–1300.

Wager TT, Hou X, Verhoest PR, and Villalobos A (2016) Central Nervous System Multiparameter Optimization Desirability: Application in Drug Discovery. *ACS Chem Neurosci* 7:767–775.

Zeng Q, Wang J, Cheng Z, Chen K, Johnstrom P, Varnas K, Li DY, Yang ZF, and Zhang X (2015) Discovery and Evaluation of Clinical Candidate AZD3759, a Potent, Oral Active, Central Nervous System-Penetrant, Epidermal Growth Factor Receptor Tyrosine Kinase Inhibitor. *J Med Chem* **58**:8200–8215.

Footnotes

This work was supported by the National Institutes of Health [Grants RO1-NS077921 RO1-NS073610 and U54-CA210180] and Strategia Therapeutics Inc. Gautham Gampa was supported by the Ronald J. Sawchuk Fellowship in Pharmacokinetics.

DMD Fast Forward. Published on February 2, 2018 as DOI: 10.1124/dmd.117.079194
This article has not been copyedited and formatted. The final version may differ from this version.

Figure legends

Fig 1. Chemical structure of (A) E6201, (B) cobimetinib, and (C) trametinib.

Fig 2. In vitro intracellular accumulation of E6201. (A)The accumulation of prazosin (Bcrp probe substrate; positive control) and E6201 in MDCKII wild-type and Bcrp1-transfected cell lines with and without Bcrp inhibitor Ko143 (0.2 μM). (B) The accumulation of E6201 and vinblastine (probe substrate for P-gp; positive control) in wild-type and MDR1-transfected cells with and without P-gp inhibitor LY335979 (1 μM). Data represent the mean ± S.D.; n = 3 for all data points. **P*< 0.05 compared with respective wild-type controls; #*P*< 0.01 compared with the untreated transfected cell line; ***P*< 0.01 compared with respective wild-type controls; ****P*< 0.001 compared with the untreated transfected cell line.

Fig 3. Pharmacokinetic profiles of E6201 in FVB wild-type, *Mdr1a/b*$^{-/-}$*, Bcrp1*$^{-/-}$*, and Mdr1a/b*$^{-/-}$ *Bcrp1*$^{-/-}$ mice following intravenous (i.v.) administration. Plasma concentrations (A), brain concentrations (B), and brain-to-plasma concentration ratios (C) of E6201 in wild-type, *Mdr1a/b*$^{-/-}$*, Bcrp1*$^{-/-}$*, and Mdr1a/b*$^{-/-}$ *Bcrp1*$^{-/-}$ mice following administration of single i.v. bolus dose of 40 mg/kg. The dashed line in (C) represents a brain-to-plasma ratio (Kp) of unity. Data represent mean ± S.D., n = 5.

Fig 4. Pharmacokinetic profiles of E6201 in FVB wild-type and *Mdr1a/b*$^{-/-}$ *Bcrp1*$^{-/-}$ mice following intraperitoneal (i.p.) administration. Plasma concentrations (A), brain concentrations (B), and brain-to-plasma concentration ratios (C) of E6201 in wild-type and *Mdr1a/b*$^{-/-}$ *Bcrp1*$^{-/-}$ mice following administration of single i.p. dose of 40 mg/kg. The dashed line in (C) represents a brain-to-plasma ratio (Kp) of unity. Data represent mean ± S.D., n = 4.

Fig 5. Pharmacokinetic profiles of E6201 in FVB wild-type mice following oral (p.o.) administration. Plasma concentrations and brain concentrations (A), and brain-to-plasma concentration ratios (B) of E6201 in wild-type mice upon single p.o. dose of 40 mg/kg. The dashed line in (B) represents a brain-to-plasma ratio (Kp) of unity. Data represent mean ± S.D., n = 4.

Fig 6. Plasma and brain unbound concentration-time profile of E6201 in FVB wild-type mice. The dashed green line represents the reported in vitro E6201 IC_{50} against SK-MEL-28 melanoma cell line (IC_{50} = 43.7 nmol/L, E6201 investigator brochure). The dashed orange line represents the free E6201 IC_{50} determined using the plasma free fraction of E6201 (fu_{plasma} = 0.026, free IC_{50} = 1.14nmol/L). Here, the assumption is that the non-specific binding of E6201 in the assay media is similar to the free fraction determined in plasma experimentally. Data represent mean ± S.D., n = 5.

DMD Fast Forward. Published on February 2, 2018 as DOI: 10.1124/dmd.117.079194
This article has not been copyedited and formatted. The final version may differ from this version.

Tables

Table 1. Free fraction (fu) for E6201 and trametinib in plasma and brain, determined by in vitro rapid equilibrium dialysis (RED) experiments. Data represent the mean ± S.D. (n = 3).

Inhibitor	Matrix	fu	fu (%)	Recovery (%)	fu_{brain}/fu_{plasma}
E6201	Plasma	0.026 ± 0.002	2.63 ± 0.18	94.04 ± 3.32	0.054
	Brain	0.0014 ± 0.0002	0.14 ± 0.02	113.20 ± 9.49	-
Trametinib	Plasma	0.0021 ± 0.0003	0.21 ± 0.03	99.90 ± 8.42	1
	Brain	0.0021 ± 0.0002	0.21 ± 0.02	106.56 ± 2.35	-

fu, free (unbound) fraction

DMD Fast Forward. Published on February 2, 2018 as DOI: 10.1124/dmd.117.079194
This article has not been copyedited and formatted. The final version may differ from this version.

Table 2. The pharmacokinetic/metric parameters of E6201 in FVB wild-type, *Mdr1a/b*$^{-/-}$, *Bcrp1*$^{-/-}$, and *Mdr1a/b*$^{-/-}$ *Bcrp1*$^{-/-}$ knockout mice following administration of single intravenous bolus dose of 40 mg/kg. Data are presented as mean or mean ± S.E.M (n=5).

	Plasma				**Brain**			
	Wild-type	*Mdr1a/b*$^{-/-}$	*Bcrp1*$^{-/-}$	*Mdr1a/b*$^{-/-}$ *Bcrp1*$^{-/-}$	Wild-type	*Mdr1a/b*$^{-/-}$	*Bcrp1*$^{-/-}$	*Mdr1a/b*$^{-/-}$ *Bcrp1*$^{-/-}$
Half-life (hr)	0.65	0.78	0.76	0.83	0.62	0.69	0.60	0.66
$AUC_{(0-t)}$ (μg*hr/mL)	10.20 ± 0.29	10.69 ± 0.75	9.89 ± 0.70	9.36 ± 0.45	27.17 ± 0.95	46.68 ± 2.51	36.78 ± 2.04	50.59 ± 3.09
$AUC_{(0-\infty)}$ (μg*hr/mL)	10.21	10.73	9.92	9.40	27.19	46.75	36.81	50.66
CL (mL/min/kg)	65.27	62.17	67.17	70.92	-	-	-	-
Vd (L/kg)	3.7	4.2	4.4	5.1	-	-	-	-
Kp ($AUC_{(0-t)}$ ratio)	-	-	-	-	2.7	4.4	3.7	5.4
Kp,uu ($AUC_{(0-t)}$ ratio)	-	-	-	-	0.14	0.24	0.2	0.29
DA	-	-	-	-	1	1.6	1.4	2

$AUC_{(0-t)}$, area under the curve from zero to the time of last measured concentration
$AUC_{(0-\infty)}$, area under the curve from zero to time infinity
CL, clearance
Vd, volume of distribution
Kp (AUC ratio), the ratio of $AUC_{(0-t,brain)}$ to $AUC_{(0-t,plasma)}$ using total drug concentrations
Kp,uu (AUC ratio), the ratio of $AUC_{(0-t,brain)}$ to $AUC_{(0-t,plasma)}$ using free drug concentrations
DA (Distribution advantage), the ratio of $Kp_{knockout}$ to $Kp_{wild-type}$

DMD Fast Forward. Published on February 2, 2018 as DOI: 10.1124/dmd.117.079194
This article has not been copyedited and formatted. The final version may differ from this version.

Table 3. The pharmacokinetic/metric parameters of E6201 in FVB wild-type and *Mdr1a/b*$^{-/-}$ *Bcrp1*$^{-/-}$ knockout mice following administration of single intraperitoneal dose of 40 mg/kg. Data are presented as mean or mean ± S.E.M (n=4).

	Plasma		**Brain**	
	Wild-type	*Mdr1a/b*$^{-/-}$ *Bcrp1*$^{-/-}$	Wild-type	*Mdr1a/b*$^{-/-}$ *Bcrp1*$^{-/-}$
Half-life (hr)	0.76	0.62	0.58	0.6
Cmax (µg/mL)	11.70 ± 2.25	18.40 ± 5.80	16.72 ± 1.36	30.75 ± 3.93
Tmax (hr)	0.25	0.25	0.5	0.5
$AUC_{(0-t)}$ (µg*hr/mL)	9.69 ± 0.73	11.73 ± 1.57	21.44 ± 1.13	44.93 ± 3.62
$AUC_{(0-\infty)}$ (µg*hr/mL)	9.73	11.75	21.46	44.99
CL/F (mL/min/kg)	68.5	56.75	-	-
Vd/F (L/kg)	4.5	3.1	-	-
Kp ($AUC_{(0-t)}$ ratio)	-	-	2.2	3.83
Kp,uu ($AUC_{(0-t)}$ ratio)	-	-	0.12	0.21
DA	-	-	1	1.75
F	0.95	-	-	-

Cmax, observed maximum concentration
Tmax, time to reach the maximum concentration
$AUC_{(0-t)}$, area under the curve from zero to the time of last measured concentration
$AUC_{(0-\infty)}$, area under the curve from zero to time infinity
CL/F, apparent clearance
Vd/F, apparent volume of distribution
Kp (AUC ratio), the ratio of $AUC_{(0-t,brain)}$ to $AUC_{(0-t,plasma)}$ using total drug concentrations
Kp,uu (AUC ratio), the ratio of $AUC_{(0-t,brain)}$ to $AUC_{(0-t,plasma)}$ using free drug concentrations
DA (Distribution advantage), the ratio of $Kp_{knockout}$ to $Kp_{wild-type}$
F (Absolute bioavailability), ratio of the dose corrected $AUC_{(0-t),ip}$ to dose corrected $AUC_{(0-t),iv}$

DMD Fast Forward. Published on February 2, 2018 as DOI: 10.1124/dmd.117.079194
This article has not been copyedited and formatted. The final version may differ from this version.

Table 4. E6201 pharmacokinetic/metric parameters in FVB wild-type mice following administration of single oral dose of 40 mg/kg. Data are presented as mean or mean ± S.E.M (n=4).

	Plasma	**Brain**
Half-life (hr)	1.37	0.98
Cmax (µg/mL)	2.44 ± 0.41	6.04 ± 1.55
Tmax (hr)	0.5	0.5
$AUC_{(0-t)}$ (µg*hr/mL)	3.94 ± 0.54	9.23 ± 1.95
$AUC_{(0-\infty)}$ (µg*hr/mL)	4.22	9.31
CL/F (mL/min/kg)	158	-
Vd/F (L/kg)	18.7	-
Kp ($AUC_{(0-t)}$ ratio)	-	2.35
Kp,uu ($AUC_{(0-t)}$ ratio)	-	0.13
F	0.39	-

Cmax, observed maximum concentration
Tmax, time to reach the maximum concentration
$AUC_{(0-t)}$, area under the curve from zero to the time of last measured concentration
$AUC_{(0-\infty)}$, area under the curve from zero to time infinity
CL/F, apparent clearance
Vd/F, apparent volume of distribution
Kp (AUC ratio), the ratio of $AUC_{(0-t,brain)}$ to $AUC_{(0-t,plasma)}$ using total drug concentrations
Kp,uu (AUC ratio), the ratio of $AUC_{(0-t,brain)}$ to $AUC_{(0-t,plasma)}$ using free drug concentrations
F (Absolute bioavailability), ratio of the dose corrected $AUC_{(0-t),po}$ to dose corrected $AUC_{(0-t),iv}$

DMD Fast Forward. Published on February 2, 2018 as DOI: 10.1124/dmd.117.079194
This article has not been copyedited and formatted. The final version may differ from this version.

Table 5. Comparison of brain distribution of MEK inhibitors in wild-type mice. Data are presented as means.

MEK inhibitor	Dose mg/kg	Kp	fu_{brain}	fu_{plasma}	Kp,uu
Trametinib	5 (iv)	0.15[a]	0.0021	0.0021	0.15
Cobimetinib[b]	10 (po)	0.32	0.0012	0.014	0.027
E6201	40 (iv)	2.66	0.0014	0.034	0.14

fu, free (unbound) fraction
Kp (AUC ratio), the ratio of $AUC_{(0\text{-}t,brain)}$ to $AUC_{(0\text{-}t,plasma)}$ using total drug concentrations
Kp,uu (AUC ratio), the ratio of $AUC_{(0\text{-}t,brain)}$ to $AUC_{(0\text{-}t,plasma)}$ using free drug concentrations
[a] Kp reported by Vaidhyanathan et al. 2014
[b] Results reported by Choo et al. 2014; Kp and Kp,uu based on plasma and brain concentrations 6 hr post dose

DMD Fast Forward. Published on February 2, 2018 as DOI: 10.1124/dmd.117.079194
This article has not been copyedited and formatted. The final version may differ from this version.

Figures

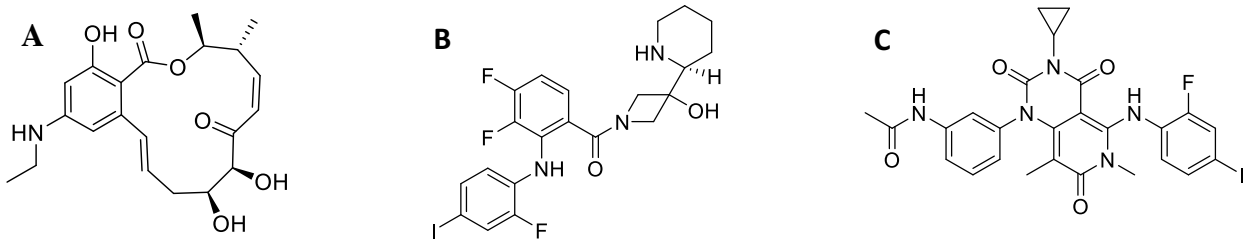

Fig 1.

DMD Fast Forward. Published on February 2, 2018 as DOI: 10.1124/dmd.117.079194
This article has not been copyedited and formatted. The final version may differ from this version.

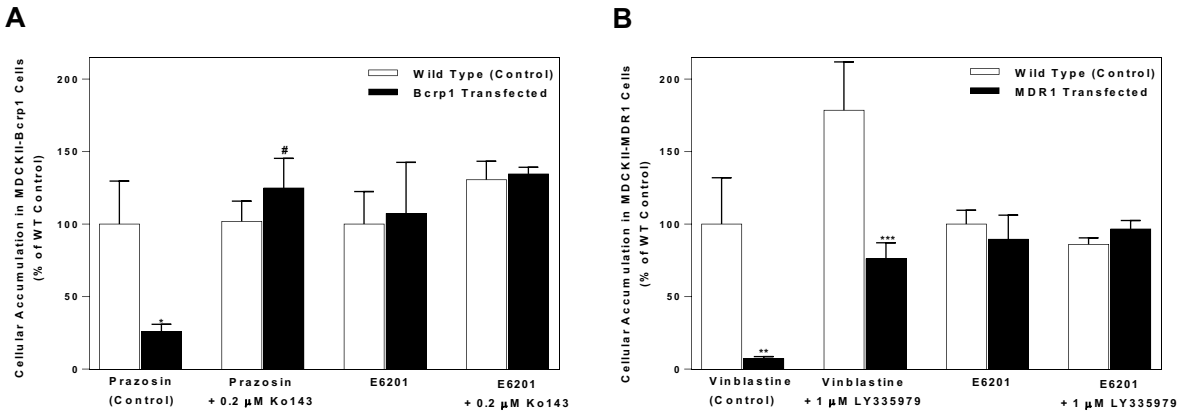

Fig 2.

DMD Fast Forward. Published on February 2, 2018 as DOI: 10.1124/dmd.117.079194
This article has not been copyedited and formatted. The final version may differ from this version.

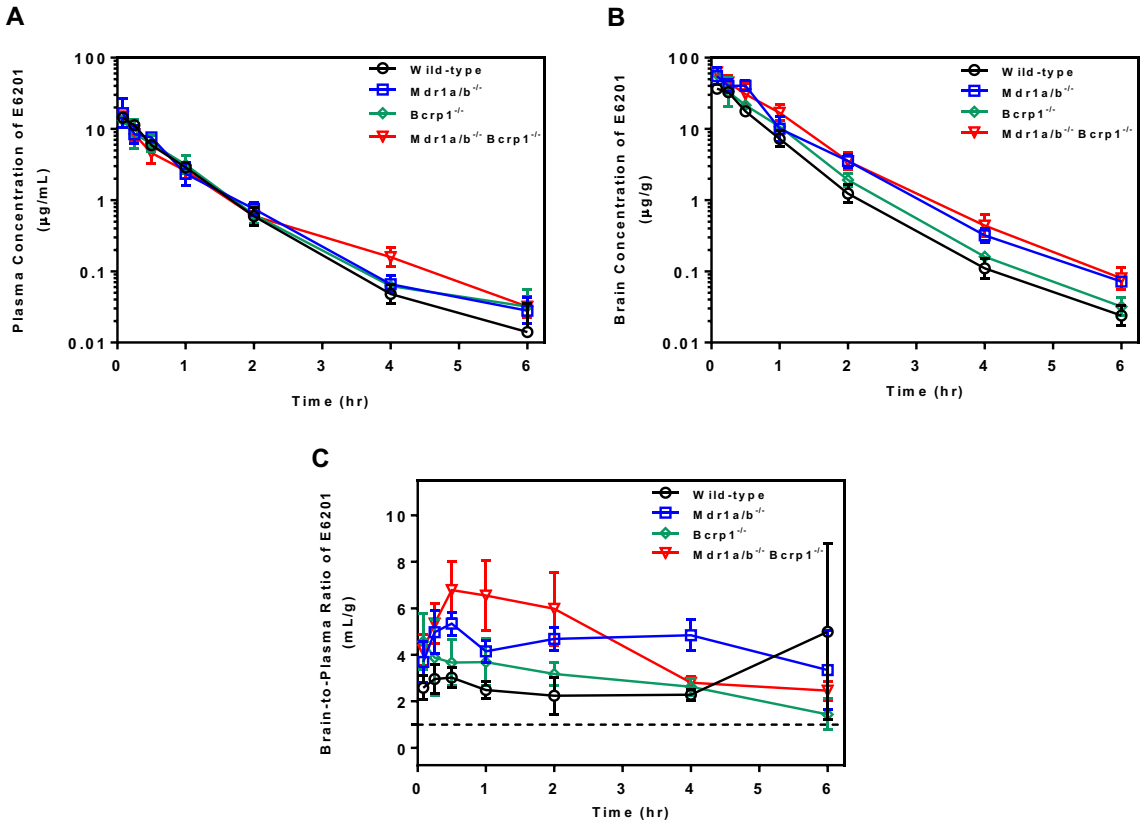

Fig 3.

DMD Fast Forward. Published on February 2, 2018 as DOI: 10.1124/dmd.117.079194
This article has not been copyedited and formatted. The final version may differ from this version.

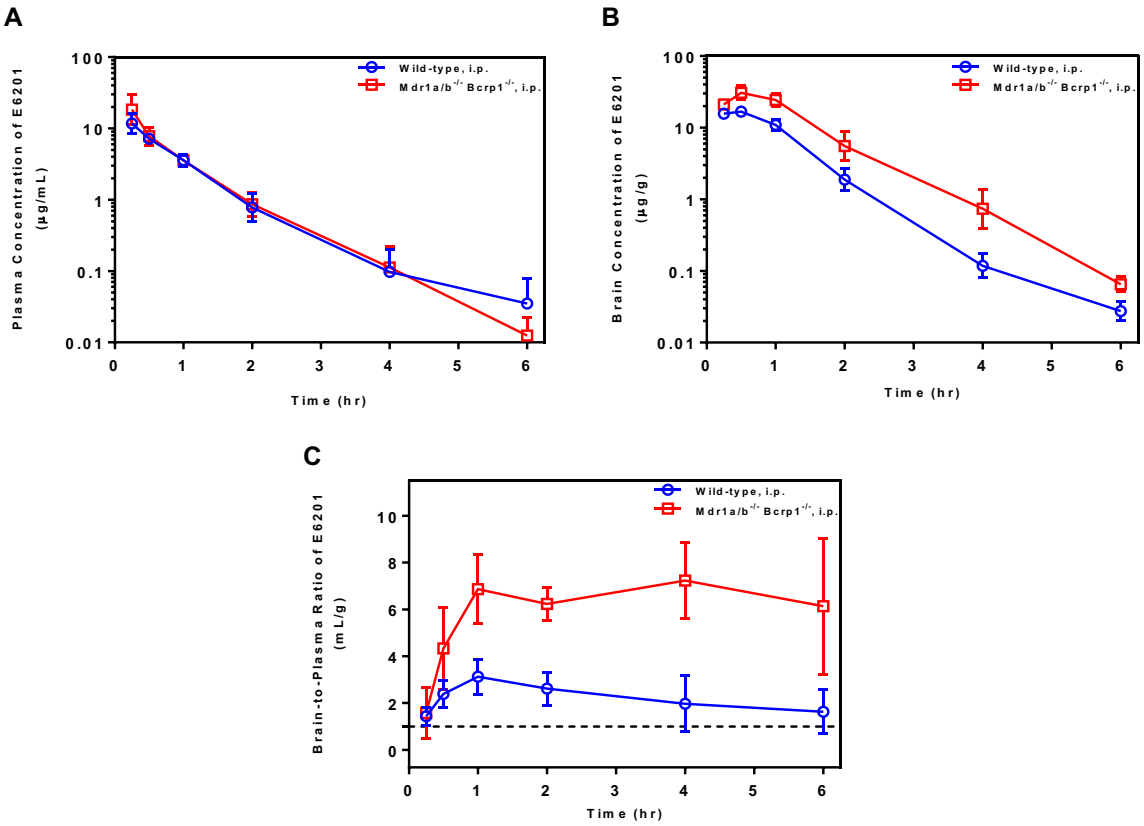

Fig 4.

DMD Fast Forward. Published on February 2, 2018 as DOI: 10.1124/dmd.117.079194
This article has not been copyedited and formatted. The final version may differ from this version.

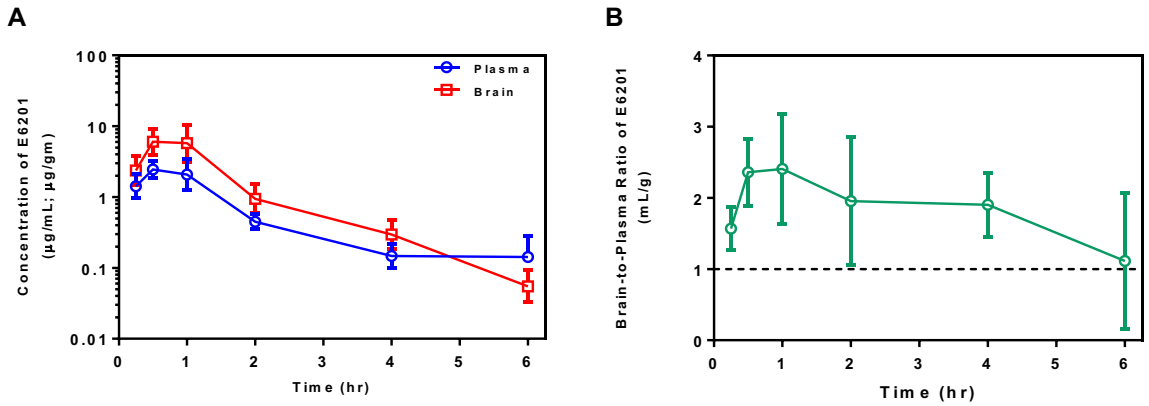

Fig 5.

DMD Fast Forward. Published on February 2, 2018 as DOI: 10.1124/dmd.117.079194
This article has not been copyedited and formatted. The final version may differ from this version.

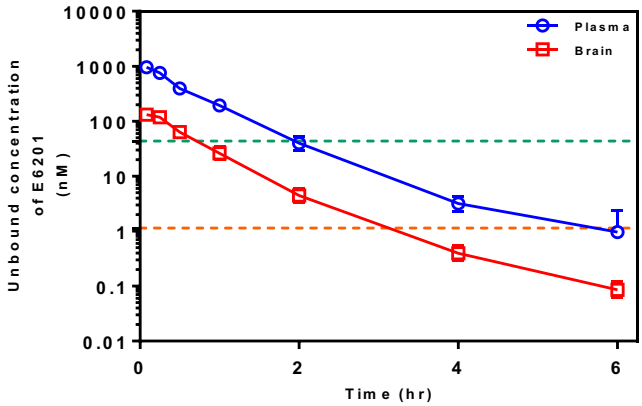

Fig 6.